Psychiatry Research: Neuroimaging 183 (2010) 126–132

Contents lists available at ScienceDirect

Psychiatry Research: Neuroimaging

journal homepage: www.elsevier.com/locate/psychresns

Detecting corpus callosum abnormalities in autism based on anatomical landmarks

Qing He[a,*], Ye Duan[a], Kevin Karsch[a], Judith Miles[b]

[a] Department of Computer Science, University of Missouri–Columbia, Columbia, MO, 65211, USA
[b] Thompson Center for Autism, University of Missouri–Columbia, Columbia, MO, 65211, USA

ARTICLE INFO

Article history:
Received 24 March 2009
Received in revised form 5 April 2010
Accepted 16 May 2010

Keywords:
Autism
Corpus callosum
Landmark
Thin-plate spline
Shape analysis

ABSTRACT

Autism is a severe developmental disorder whose neurological basis is largely unknown. The aim of this study was to identify the shape differences of the corpus callosum between patients with autism and control subjects. Anatomical landmarks were collected from midsagittal magnetic resonance images of 25 patients and 18 controls. Euclidean distance matrix analysis and thin-plate spline analyses were used to examine the landmark forms. Point-by-point shape comparison was performed both globally and locally. A new local shape comparison scheme was proposed which compared each part of the shape in its local coordinate system. Point correspondence was established among individual shapes based on the inherent landmark correspondence. No significant difference was found in the landmark form between patients and controls, but the distance between the interior genu and the posterior-most section was found to be significantly shorter in patients. Thin-plate spline analysis showed significant group differences between the landmark configurations in terms of the deformation from the overall mean configuration. Significant global shape differences were found in the anterior lower body and posterior bottom, and there was a local shape difference in the anterior bottom. This study can serve as both a clinical reference and a detailed procedural guideline for similar studies in the future.

1. Introduction

Autism is a severe developmental disorder characterized by social deficits, impaired communication, and restricted and repetitive behavior patterns (American Psychiatric Association, 2000). Magnetic resonance imaging (MRI) has found inconsistent results regarding the abnormalities of brain structures in autism. The inconsistency may be due to factors such as the sample size, subject age and gender. However, heterogeneity within the autism diagnosis can significantly obscure the genetic basis of the disorder (Miles et al., 2005).

The corpus callosum (CC) is the major commissural pathway between the brain hemispheres and plays an integral role in relaying sensory, motor, and cognitive information from homologous regions in the two hemispheres. Many studies have reported abnormalities of the CC in autism. Quantitative morphologic assessment of individual brain structures is often based on volumetric measurements and shape analysis. Volume comparison gives global information about the size difference between pathological and healthy structures, but no local shape difference is revealed. Early works focused mostly on the area of the CC on the midsagittal slice (e.g., Piven et al., 1997; Hardan et al., 2000), and most of them found reductions in the size of different sub-regions of the CC in autism. Shape analysis, on the other hand, can precisely locate morphologies at any location on the brain structure. However, point correspondence among individual shapes is a crucial and difficult problem. Studies by Vidal et al. (2006) and He et al., (2008) both found the anterior and posterior portions of the CC were more inward in autism. Point correspondence was established globally across the entire shape. Note that their shape correspondence was based on 2D contours of the CC on sagittal MR images, because the shape characteristics of the of the CC can be sufficiently reflected by the sagittal view.

Landmark-based shape analysis has been popular in neuroanatomical research because of its convenience and effectiveness in obtaining shape information. Landmarks are usually determined by anatomical prominences of the biological structure of interest. Euclidean distance matrix analysis (EDMA) and thin-plate spline (TPS) analysis are two common ways to examine the landmarks. EDMA uses landmark coordinate data to calculate all pairwise distances between landmarks (Burrows et al., 1999). It is invariant to the coordinate system, which makes it biologically and statistically advantageous (Theodore and Richtsmeier, 1998). For example, it was used to analyze sex-related differences in the inter-landmark distances of the CC (Ozdemir et al., 2007). TPS (Bookstein, 1989) has been widely used to compare landmark configurations (Ozdemir et al., 2007; Bookstein et al., 2001; Fink and Zelditch, 1995; Lapeer and Prager, 2000; Rosas and Bastir, 2002). The fundamental principle of TPS is the comparison of two different shapes by deforming one shape to the other. The expansion factors can be used as a measurement of the deformation (Bookstein, 1991).

* Corresponding author. 201 Engineering Building West, Columbia, MO 65211, USA. Tel.: +1 573 882 3951; fax: +1 573 882 8318.
E-mail address: qhgb2@mizzou.edu (Q. He).

0925-4927/$ – see front matter © 2010 Elsevier Ireland Ltd. All rights reserved.
doi:10.1016/j.pscychresns.2010.05.006

Although the above landmark analyses can reveal some shape information, shape morphologies at non-landmark locations cannot be detected. In this study, we conducted both traditional landmark analyses and a landmark-guided shape comparison, in order to examine the abnormalities of the CC in autism. A configuration of landmarks was identified in brain MRI midsagittal sections based on a predefined criterion (Ozdemir et al., 2007). In the traditional analyses, we performed the aforementioned EDMA and TPS procedures. In the landmark-guided shape comparison, we aimed at finding the morphology at every location on the shape. Point correspondence was established based on the landmark correspondences, and statistical methods were used to compare two groups of shapes (autism vs. control) at every location in the global shape comparison. In addition, a new local shape comparison was proposed that assessed each part of the shape in its local coordinate system. Each of the above three analyses examined the shape morphology from a different perspective.

2. Materials and methods

2.1. Subjects

The study was conducted on patients with autism and the control subjects. Twenty-five children with autism were recruited from the Thompson Center for Autism and Neurodevelopmental Disorders. All patients came from families who had come to the Thompson Center and gone through our standard diagnostic protocol (Autism Diagnostic Interview - Revised, Autism Diagnostic Observation Schedule, cognitive evaluation, genetic assessment). Children with disorders known to cause an autism phenotype such as Fragile X, chromosome abnormalities or severe prematurity with brain damage, children with IQs less than 50 and children with premature puberty were excluded. To maximize homogeneity, children in this autism group were limited to individuals with no history of seizures, abnormal brain EEGs, or abnormal MRIs.

Eighteen control subjects were recruited from the community under the regulations of the Thompson Center control subject recruitment protocol. The control group of typically developing children was matched for gender, age and ancestry. They underwent a short intake history to rule out significant language, cognitive or social delays. Children receiving special education with an IEP, diagnosed and treated symptoms of attention deficit/hyperactivity disorder and other childhood psychiatric disorders, and children with a sibling diagnosed with autism were excluded.

Table 1 summarizes the demographic characteristics of the autistic patients and comparison controls. Student's t-test was used to compare the ages, and the χ^2 test was used to compare the gender ratios. There is no significant difference between the two groups in terms of age, gender and race.

This study was approved by the Health Sciences Institutional Review Board. The parents or legal guardians of all subjects provided written consent for participation in this study, while the subject provided voluntary assent.

Table 1
Demographic characteristics of autistic patients and controls.

Measures	Patients	Controls	Test statistics	P-value
Age (mean ± std)	6.86 ± 2.87 (Range 3.6~12.8)	8.44 ± 4.34 (Range 4.5~14.2)	$t = 0.861$	0.197
Gender (M:F)	20:5	14:4	$\chi^2 = 0.030$	0.975
Race	All Caucasians	All Caucasians		

2.2. MRI acquisition and processing

Axial, coronal and sagittal T1-weighted images were acquired using the Siemens Symphony 1.5 T scanner with the following parameters: TR = 35 ms, NEX = 1, flip-angle = 30°, thickness = 1.5 mm, field of view = 22 cm, matrix = 512 × 512. Sedations were performed if needed on some of the subjects based on our autism anesthesia protocol. The 16-bit MR data were compressed to 8 bits by linearly rescaling the voxel intensities. Any voxel whose intensity was below the 2nd percentile was set to 0, and any voxel whose intensity was above the 98th percentile was set to 255. The remaining voxel intensities were then linearly interpolated between these two extremes to ensure that all data points fell within the 8-bit scale. The data were aligned with the stereotactical coordinate system and re-sliced to isotropic voxels of 1 mm^3 using Slicer (www.slicer.org).

2.3. CC segmentation and landmark collection

From the sagittal planes, the midsagittal section that most clearly displayed the cerebral aqueduct, CC, and superior colliculus was selected manually (Ozdemir et al., 2007). From the midsagittal image, the CC was segmented using a semiautomatic method (He et al., 2007). Three mouse clicks were required and the segmentation was then performed automatically. In order to ensure the accuracy of the segmentation, we allowed manual adjustment of the segmentation result if it did not comply with the true CC boundary. Generally this method worked well on most data sets, and the need for manual adjustment was rare. The accuracy of this method was validated (He et al., 2007). The segmentation was performed by the same trained expert for all the data. The resulting contour was represented as a sequential point list.

After the CC contour of each subject was extracted, the contours were aligned in order to remove the shape differences due to translation, scaling and rotation. The centroid of each shape was calculated as the mean coordinates of the points on the contour, and the shape was translated by the centroid coordinates so that the new centroid was at the origin. Then each shape was scaled by its normalized centroid size defined as follows:

$$s = \sqrt{\frac{1}{N}\sum_{i=1}^{N}\left(x_i^2 + y_i^2\right)} \tag{1}$$

where N is the number of points on the contour. The centroid size obtained from the scaling step is the only size measurement that is uncorrelated with shape variation (Bookstein, 1991). Therefore, our analysis reveals a pure shape difference without the effect of size. The rotation difference is then removed by aligning the principal axes of each shape to those of a template shape which can be randomly selected from the entire group of contours (Dalal et al., 2007).

Nine anatomical landmarks were identified on each of the aligned CC shapes (Fig. 1). Anatomical landmarks are biologically meaningful loci that can be repeatedly located with high accuracy and precision

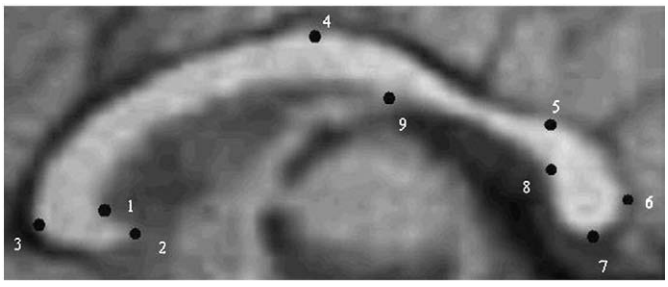

Fig. 1. Landmarks of the CC.

Table 2
Landmark definitions.

Landmarks	Definitions
1	Interior angle of genu
2	Tip of genu
3	Anterior most of CC
4	Topmost of CC
5	Splenium topmost point
6	Posterior most of CC
7	Bottommost of splenium
8	Interior notch of splenium
9	CC-fornix junction

(Richtsmeier et al., 1995). We followed the landmark definition in (Ozdemir et al., 2007), which included extreme points or terminals and maxima of curvature (Table 2). All landmarks were manually identified by a single rater. Intra-rater and inter-rater reliability of landmark selection was tested using the method described in Ercan et al. (2008). Two raters each performed the landmark selection twice, and G-coefficients between two landmark sets from the same rater (2 pairs) and from two different raters (4 pairs) were calculated. A G-coefficient close to 1 indicates high intra/inter-rater reliability. The minimum G-coefficient for all six pairs of landmark sets was 0.994, which indicated high reliability of the landmark selection.

2.4. Form difference analysis by EDMA

In this analysis the shape change was measured in terms of the overall landmark configuration. Euclidean distances were calculated between every pair of landmarks, leading to a form matrix for each shape (Burrows et al., 1999). The k landmarks had $k(k-1)/2$ inter-landmark distances. Since the form matrix is symmetric, a form vector of length $k(k-1)/2$ can be used to describe the matrix. Box's M test (Dryden and Mardia, 1998) was performed to test the homogeneity of the variance. The EDMA I method was used if there were existing homogeneities of variance–covariance matrices; otherwise, EDMA II method was preferred for shape analysis.

We adopted the EDMA I method because the hypothesis of homogeneity of variance could not be rejected ($P=0.95$). We performed statistical tests on the null hypothesis that the two groups of shapes did not differ in form (Burrows et al., 1999). In brief, the average form vector was computed within each group, and the ratio of the two average form vectors was the form difference vector. The raw test statistic was computed from the maximum value (max) and the minimum value (min) of the form difference vector, which was $T_0=\max/\min$. A permutation test was used to find the statistical significance of the difference between the two form vectors. In this procedure, a bootstrap was used to generate M permutated samples, and thus M test statistics (T^*) can be computed in the same fashion as T_0. The percentage of T^* that was greater than T_0 was the P-value. A significant level of 0.05 was selected and $M=1000$ in our experiment.

We also performed traditional t-tests on each inter-landmark distance under the null hypothesis that each distance was the same in the two groups. Since only a small number ($9^*8/2=36$) of distances were tested simultaneously, the Bonferroni procedure (Shaffer, 1995) was used to adjust each P-value for multiple comparison.

2.5. Shape deformation analysis by TPS

TPS (Bookstein, 1989) describes the deformation by a mapping function $f(x,y)=[f_x(x,y),f_y(x,y)]$ which maps the location (x,y) to a new location $[f_x,f_y]$. Each of the functions f_x and f_y has the form:

$$f_*(x,y) = a_0 + a_x x + a_y y + \sum_{i=1}^{n} w_i \phi(||(x_i,y_i)-(x,y)||) \quad (2)$$

where $\phi(r)=r^2\log r^2$,(x_i, y_i) are the landmark coordinates on the starting form, * can be x or y, and n is the number of landmarks. Given that $f(x_i,y_i)=v_i$ where v_i is the corresponding landmark on the target form, the coefficients a_0, a_x, a_y, w_i can be solved from a linear equation.

Define the following matrices

$$K=\begin{bmatrix} 0,\phi(r_{12}),\ldots,\phi(r_{1n}) \\ \phi(r_{21}),0,\ldots,\phi(r_{2n}) \\ \ldots\ldots\ldots\ldots\ldots\ldots \\ \phi(r_{n1}),\ldots\ldots,0 \end{bmatrix}_{n\times n} \quad P=\begin{bmatrix} 1,x_1y_1 \\ 1,x_2y_2 \\ \ldots\ldots\ldots \\ 1,x_ny_n \end{bmatrix}_{n\times 3}$$

$$L=\begin{bmatrix} K,P \\ P^T,O \end{bmatrix}_{(n+3)\times(n+3)} \quad Y=\begin{bmatrix} \vec{v}_1 \\ \vec{v}_2 \\ \ldots \\ \vec{v}_n \\ O \end{bmatrix}_{(n+3)\times 2}$$

where O is a matrix of zeros whose size depends on the parent matrix it is in and $r_{ij}=||(x_i,y_i)-(x_j,y_j)||$. The two columns of the matrix $L^{-1}Y$ are the coefficients in the functions f_x and f_y, respectively. The $2n$ coefficients w_i (n coefficients in each direction) correspond to the non-uniform (non-affine) transformation. The expansion factor at each landmark can be computed from the Jacobian of w_i with respect to the transformed landmarks (Bookstein, 1991).

Two types of shape deformation were calculated. The first type was the deformation from the mean landmark form of the controls to that of the patients. The second type was the deformation from the overall mean landmark form (both patients and controls) to the mean forms of the patients and the controls, respectively. For each type we used the data analysis package PAST (Hammer et al., 2001) to calculate the expansion factors and display the deformation grid.

The overall mean landmark form was also deformed to the landmark set of each individual subject, and multivariate statistical analysis was used to compare the non-uniform coefficients w_i between patients and controls. Specifically, Hotelling T^2 two-sample test was performed separately on the coefficient vectors in x direction ($n-D$), the coefficient vectors in y direction ($n-D$) and the concatenated coefficient vectors of both directions ($2n-D$). A positive, larger T^2 corresponds to a smaller P-value, which indicates more significant group difference in the landmark deformation.

2.6. Landmark-guided shape comparison

In this section, shape difference was examined at every location on the contour. Two types of shape comparison were conducted: one in the global coordinates and one in the local coordinates. Point correspondence among individual shapes must be established before any shape comparison. Previous methods on shape correspondence have been proposed such as shape contexts (Belongie et al., 2002) and landmark sliding (Dalal et al., 2007). Most of them try to use some global optimization algorithm to find the correspondence between two shapes without any consideration about the object that the shape represents. The problem is that meaningful points may not be matched among individual shapes. For example, one cannot guarantee that an anatomical landmark on one CC shape is also matched to the same landmark on the other CC shape. We address this problem by using the landmarks as guidance for shape correspondence. Since the landmarks used in this study represent certain anatomical features on the CC shape, we assume that they are already corresponded. The landmarks divide the contour into several segments, and thus the segments terminated by the same two landmarks are corresponded among different shapes. The rest task is to find the point correspondence each segment, which becomes much simpler since each segment is a simple open contour and the two terminal points (which are landmarks) are already corresponded. Although more complex algorithms can be used for the correspondence of each segment, a simple uniform sampling can serve this purpose without much difference in the results. The

sampling can be implemented by axis parameterization in which the sampled points are equally spaced along the axis defined by the two terminal landmarks, or by arc-length parameterization in which the points are equally spaced along the contour. These two methods have similar results when the contour is close to a straight line. For axis parameterization, we require the contour segment to be a single valued function of the points on the axis in order to obtain a unique point on the contour at each sampling point on the axis. The contour segments defined by our landmarks satisfy this requirement, and there is no global curvature extreme within each segment because the landmarks already cover the curvature extremes on the contour. Therefore, we used axis parameterization since it was simple. Fig. 2(a) illustrates the uniform sampling on one segment. For each segment, we sampled the same number of points on different shapes, so that these points were corresponded by their indices. For simplicity, we ignored landmark 9 in the sampling process because the segment between landmarks 1 and 8 already satisfied the single value condition. In order to keep the point density the same along the entire shape contour, we set the number of sampled points on each segment proportional to the average length of this segment across different shapes. Fig. 2(b) shows the resulting point correspondence between two CC contours. The point correspondence can be used for both global comparison and local comparison.

In the global comparison, aligned CC shapes (Section 2.3) were compared point by point across the whole contour. Since each point coordinate is a 2D vector, the Hotelling T^2 two-sample metric was used again. Each raw P-value obtained from the test statistic T^2 was an optimistic estimation because the comparisons were made at hundreds of CC contour points. It was important to control the P-values for the multiple comparison problem. Non-parametric permutation tests (Pantazis et al., 2004) and False Discovery Rate estimate (FDR) (Hochberg and Benjamini, 1995) were typically used for P-value correction. We adopted FDR because it provides an interpretable and adaptive criterion with higher power, and also is computationally efficient (Styner et al., 2006). The FDR method allows the false positive to be within a small proportion α ($\alpha = 0.01$ in our experiment).

In the local comparison, we focused on the group difference in each part of the CC shape instead of the whole shape. Each contour segment was compared in its local coordinate system as shown in Fig. 2(a). The x-axis was the line connecting the two terminal landmarks, and we scaled the distance between the two terminal landmarks to 1. In this way the same segments across difference shapes were aligned by a common local coordinate system. Since our uniform sampling for point correspondence was based on the x-axis, the corresponding points had the same x coordinates in their local coordinate system. For each segment, we compared the y-coordinates of the points between the two groups using t-tests followed by FDR correction. While the global comparison gives the group difference of the whole shape regardless of the segments, the local comparison gives the shape difference with regard to each part of the shape.

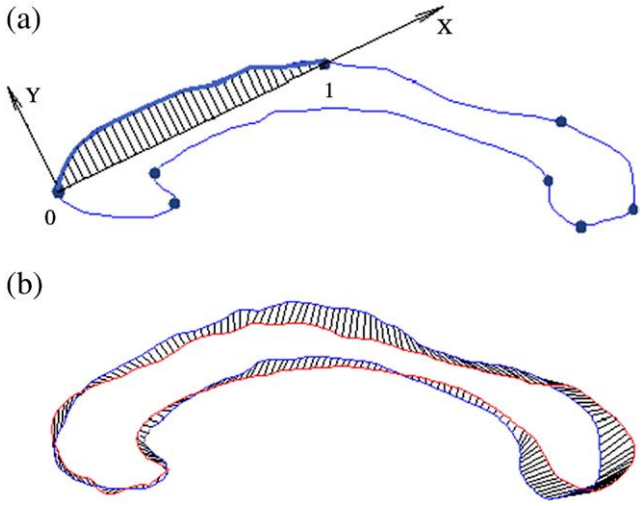

Fig. 2. (a) Uniform sampling and local coordinate system on one segment of the CC contour. (b) The correspondence between two CC contours.

3. Results

3.1. Form difference of landmarks

In EDMA analysis, no significant difference was found in the landmark form between the two groups of shapes ($P = 0.41$). In the tests of individual distances, most of the inter-landmark distances did not show significant differences between the two groups after P-value correction. The only significant difference was found in the distance from landmarks 1 to 6 ($P = 0.0006$). Fig. 3 shows the mean landmark configurations of the patients and the controls overlaid on the mean shape of the CC. The distance 1–6 was longer in the control shape than in the patient shape.

3.2. Shape deformation

Fig. 4 shows the TPS transformation grid along with the expansion factors of the transformation to each group from the overall mean. In the deformation from overall mean to the patients (Fig. 4(a)), landmark 3 (anterior most) exhibits expansion and all other landmarks exhibit shrinking. Landmark 7 (posterior bottom) has the largest shrinking. In the deformation from overall mean to the controls (Fig. 4(b)), landmark 3 (anterior most) exhibits shrinking and all others exhibit expansion. Landmark 7 has the largest expansion. The deformation from the controls to the patients (Fig. 4(c)) is similar to the deformation in Fig. 4(a) except the expansion and shrinking are stronger. Landmark 7 again has the largest shrinking.

Hotelling T^2 test indicated that there was a significant difference between patients and controls in the concatenated deformation coefficients ($P = 0.01$), but no significant difference in the coefficients of x ($P = 0.09$) or y direction ($P = 0.9$) alone.

3.3. Local shape differences

Fig. 5(a) shows the average CC shapes of the two groups, providing a descriptive visualization of the shape difference between the two groups. The CC of the patients is more inward at both ends, resulting in a shorter distance in anterior–posterior length which is consistent with the results in Section 3.1. Note that the difference in the length does not reflect the size because we have removed the size difference in our spatial alignment. It is rather due to the different bending degrees of the CC body. Fig. 5(b) and (c) shows the raw and corrected significance maps of the global shape comparison (significance level = 0.05). The raw P-values suggest significant shape difference in the anterior most and top, anterior lower body and posterior, while the corrected P-values retain significant differences in the anterior lower body and posterior bottom. This is consistent with the results in

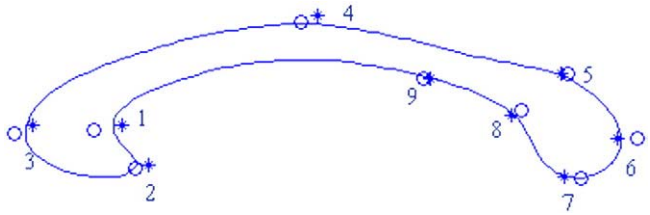

Fig. 3. Overlaid mean landmark configurations of the patients (*) and the controls (o) on the overall mean shape. (a) Overall mean to patients. (b) Overall mean to controls. (c) Controls to patients.

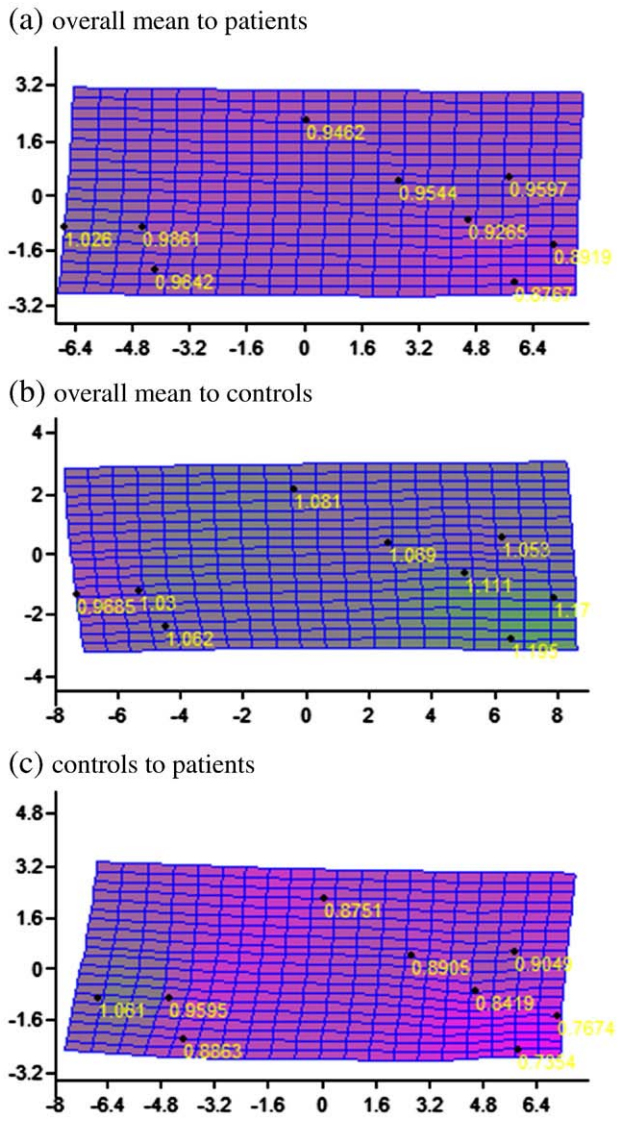

Fig. 4. TPS transformation grids and the expansion factor at each landmark.

Section 3.2 where the posterior bottom of the shape for the patient group shows severe shrinking relative to the control shape. Fig. 5(d) and (e) shows the raw and corrected significance maps of the local shape comparison, where landmarks are highlighted in a different color. There is a significant shape difference in the anterior bottom and posterior lower body in the raw *P*-values, and the corrected *P*-values retain the significance in the anterior bottom and part of the posterior lower body (isthmus). Both anterior bottom and isthmus bottom show different bending degrees between patients and controls, which causes the local shape difference.

4. Discussion

Most previous studies found reduced size in the CC in autism, but the results are inconsistent with regard to CC sub-regions. For example, Piven et al. (1997) reported reductions in the size of the body and posterior regions of the CC in autistic patients, Hardan et al. (2000) found significant differences in anterior regions, and Vidal et al. (2006) found reductions in the genu and the splenium. A recent study (Duan et al., 2009) measured the oriented bounding rectangle of the CC and found the anterior–posterior length is shorter in autism. Shape analysis (Vidal et al., 2006) found the anterior and posterior of the CC were less projected in autism, which also indicated a shorter anterior–posterior length.

Local shape analysis has gained more interest recently due to its potential to locate shape morphologies. However, only a few studies have conducted local shape analysis of the CC in autism. Landmark-based methods have been popular in shape analysis due to the belief that evaluating general form differentiation in the shape by using neuroanatomical landmarks is most relevant (Ozdemir et al., 2007). In this study, we performed traditional landmark-based analyses using the EDMA and TPS methods to examine the shape abnormalities of the CC in autism. Moreover, we used the anatomical landmarks as a guidance to establish the point correspondence among individual shapes, thus facilitating the following shape comparison. Every point location was compared in both global and local shape comparisons so that more details of the shape abnormalities could be revealed. To our knowledge, this study was the first to use landmark-based methods to analyze the CC abnormalities in autism, and the local shape comparison had not been done before.

Our analysis permits some insight into the callosal functions potentially involved in the pathology of autism. The connections across

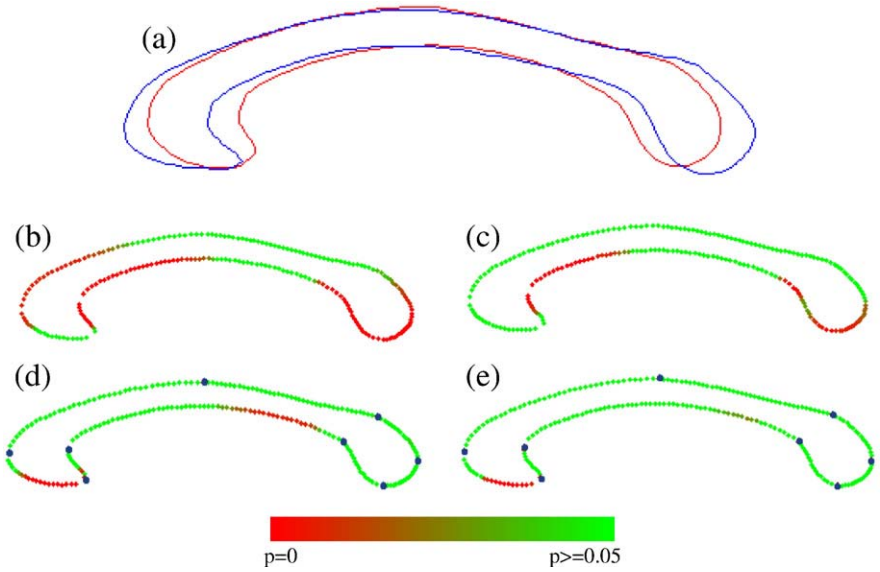

Fig. 5. (a) Average shapes of the CC (red: patients; blue; controls). (b) Raw significance map of the global comparison. (c) Corrected significance map of the global comparison. (d) Raw significance map of the local comparison. (e) Corrected significance map of the local comparison (landmarks are shown as blue dots in (d) and (e)).

the corpus callosum are topographically organized where the relay of sensory, motor and cognitive information is transmitted from two cerebral hemispheres. Existing findings have suggested the complexity of the callosal connectivity. For example, Moses et al. (2000) examined the regional size reduction of the CC in children with focal lesions, and confirmed the cortico-callosal topography documented in adult persons and nonhumans. It also suggested limits to developmental neuroplasticity subsequent to perinatal brain injury. Aboitiz et al. (1992) reported that primary and secondary sensory information was transmitted via large diameter callosal fibers and higher-order sensory and cognitive information was transmitted through small diameter fibers. There are different representations of large and small diameter fibers in different callosal channels (Aboitiz et al., 1992). Anterior callosal regions may be involved in the transmission of cognitive information (Clarke et al., 1998). The isthmus is where the callosal motion fibers cross through (Wahl et al., 2007), and it has been demonstrated to connect myelinated fibers from posterior language regions and auditory association areas (Clarke and Zaidel, 1994). Local shape differences are found in these areas in our study, which may be associated with the aberrant cognition and impaired verbal communication in autism. Posterior callosal regions are involved in transmitting sensory information (Clarke et al., 1998), and autistic patients often have extreme sensory issues (hypersensitivity or hyposensitivity) which may be related to the more inward posterior of the patients found in our study.

The results reported in this article need to be interpreted with caution. We include both males and females in our subjects, which may overlook the gender difference of the CC (Ozdemir et al., 2007). However, due to the unbalanced male-to-female ratio (4:1) in autism, it is difficult to conduct separate experiment in female patients because of the sample size. We therefore use a matching ratio of males to females in the control subjects. The sample size in this study is relatively small, which may affect the statistical results. Further study on a larger sample size will be conducted when more data are available.

The contribution of this study is two-fold. First, the findings of this study provide some insight into the pathology of autism related to the functions of the CC, although further studies need to be performed to confirm the results. Secondly, the procedures of our analysis can be applied to similar studies of other brain structures. The CC is a special brain structure whose shape can be characterized by a 2D contour. Generalizing our methods to other 2D biological shapes is straightforward since anatomical landmarks on 2D shapes are usually distinct to visualize and manually identify. However, most brain structures are naturally 3D, which adds more difficulty to the shape analysis. Manually identifying anatomical landmarks on a 3D mesh is non-trivial and less accurate, and some automatic or semiautomatic methods for 3D landmark localization have been developed recently which demonstrate their potential in clinical application (Liu et al., 2008; Worz and Rohr, 2006). Point correspondence among 3D shapes is even more challenging, and most existing methods do not explicitly consider anatomical landmarks (Dalal et al., 2007; Styner et al., 2006). We believe that anatomical landmarks can still serve as guidance for establishing point correspondence among 3D shapes. An ongoing study is being carried out which extends our method in Section 2.6 to the case of 3D shapes. Therefore, with some modifications, our landmark-based analysis framework can still be a promising method for 3D shapes.

In conclusion, this study found global shape differences caused by different bending degrees of the CC body, and local shape differences in the anterior bottom of the CC between the autism and control groups. These abnormalities of the CC may be related to the cognitive, sensitive and motor deficiencies in autism. This study can serve as both clinical reference and guidance for similar studies.

Acknowledgments

This work is supported in part by a NIH pre-doctoral training grant for Clinical Biodetectives, a Thompson Center Research Scholar fund, the Department of Defense Autism Concept Award, and the NARSAD Foundation Young Investigator Award.

References

Aboitiz, F., Scheibel, A.B., Fisher, R.S., Zaidel, E., 1992. Fiber composition of the human corpus callosum. Brain Research 598, 143–153.
American Psychiatric Association, 2000. Diagnostic and Statistical Manual of Mental Disorders, 4th ed. Text revision. APA, Washington DC. text revision.
Belongie, S., Malik, J., Puzicha, J., 2002. Shape matching and object recognition using shape contexts. IEEE Transactions on Pattern Analysis and Machine Intelligence 24 (4), 509–522.
Bookstein, F.L., 1989. Principal warps: thin-plate splines and the decomposition of deformations. IEEE Transaction on Pattern Analysis and Machine Intelligence 11, 567–585.
Bookstein, F.L., 1991. Morphometric Tools for Landmark Data. Cambridge University Press, Cambridge.
Bookstein, F.L., Sampson, P.D., Streissguth, A.P., Connor, P.D., 2001. Geometric morphometrics of corpus callosum and subcortical structures fetal-alcohol-affected brain. Teratology 64, 4–32.
Burrows, A.M., Richtsmeier, J.T., Mooney, M.P., Smith, T.D., Losken, H.W., Siegel, M.I., 1999. Three-dimensional analysis of craniofacial form in a familial rabbit model of nonsyndromic coronal synostosis using Euclidean distance matrix analysis. The Cleft Palate-Craniofacial Journal 36, 196–206.
Clarke, J.M., McCann, C.M., Zaidel, E., 1998. The corpus callosum and language: anatomical–behavioral relationships. In: Beeman, M., Chiarello, C. (Eds.), Right Hemisphere Language Comprehension: Perspectives from Cognitive Neuroscience. Lawrence Erlbaum, Mahwah, NJ, pp. 27–50.
Clarke, J.M., Zaidel, E., 1994. Anatomical–behavioral relationships: corpus callosum morphometry and hemispheric specialization. Behavioral Brain Research 64, 185–202.
Dalal, P., Munsell, B.C., Wang, S., Tang, J., Kenton, O., Ninomiya, H., Zhou, X., Fujita, H., 2007. A Fast 3D Correspondence Method for Statistical Shape Modeling. IEEE Conference on Computer Vision and Pattern Recognition, Minneapolis.
Dryden, I.L., Mardia, K.V., 1998. Statistical Shape Analysis. John Wiley and Sons, New York.
Duan, Y., He, Q., Yin, X., Gu, X., Karsch, K., Miles, J., 2009. Detecting corpus callosum abnormalities in autism subtype using planar conformal mapping. Communications in Numerical Methods in Engineering 26 (2), 164–175.
Ercan, I., Ocakoglu, G., Guney, I., Yazici, B., 2008. Adaptation of generalizability theory for inter-rater reliability for landmark localization. International Journal of Tomography & Statistics 9 (S08), 51–58.
Fink, W.L., Zelditch, M.L., 1995. Phylogenetic analysis of ontogenetic shape transformations: a reassessment of the piranha genus pygocentrus (teleostei). System Biology 44 (3), 343–360.
Hammer, Ø., Harper, D.A.T., Ryan, P.D., 2001. PAST: Paleontological Statistics Software Package for Education and Data Analysis. Palaeontologia Electronica 4 (1) 9 pp. http://palaeo-electronica.org/2001_1/past/issue1_01.htm.
Hardan, A.Y., Minshew, N.J., Keshavan, M.S., 2000. Corpus callosum size in autism. Neurology 55, 1033–1036.
He, Q., Duan, Y., Miles, J.H., Takahashi, T.N., 2007. A context-sensitive active contour for image segmentation. International Journal of Biomedical Imaging 2007. doi:10.1155/2007/24826 Article ID 24826.
He, Q., Duan, Y., Miles, J.H., Takahashi, N., 2008. Abnormalities of the corpus callosum in autism subtype. International Journal of Functional Informatics and Personalized Medicine 1 (1), 103–110.
Hochberg, Y., Benjamini, Y., 1995. Controlling false discovery rate: a practical and powerful approach to multiple testing. Journal of the Royal Statistical Society: Series B 57, 289–300.
Lapeer, R.J.A., Prager, R.W., 2000. 3D shape recovery of a newborn skull using thin-plate splines. Computerized Medical Imaging and Graphics 24, 193–204.
Liu, J., Gao, W., Huang, S., Nowinski, W.L., 2008. A model-based, semi-global segmentation approach for automatic 3-D point landmark localization in neuroimages. IEEE Transactions on Medical Imaging 27 (8), 1034–1044.
Miles, J.H., Takahashi, T.N., Bagby, S., Sahota, P.K., Vaslow, D.F., Wang, C.H., Hillman, R.E., Farmer, J.E., 2005. Essential vs complex autism: definition of fundamental prognostic subtypes. American Journal of Medical Genetics Part A 135, 171–180.
Moses, P., Courchesne, E., Stiles, J., Trauner, D., Egaas, B., Edwards, E., 2000. Regional size reduction in the human corpus callosum following pre- and perinatal brain injury. Cerebral Cortex 10 (12), 1200–1210.
Ozdemir, S.T., Ercan, I., Sevinc, O., Guney, I., Ocakoglu, G., Aslan, E., Barut, C., 2007. Statistical shape analysis of differences in the shape of the corpus callosum between genders. The Anatomical Record 290, 825–830.
Pantazis, D., Leahy, R.M., Nichol, T.E., Styner, M., 2004. Statistical surface-based morphometry using a non-parametric approach. International Symposium on Biomedical Imaging, pp. 1283–1286. April.
Piven, J., Bailey, J., Ranson, B.J., Arndt, S., 1997. An MRI study of the corpus callosum in autism. The American Journal of Psychiatry 154, 1051–1056.
Richtsmeier, J., Paik, C., Elfert, P., Cole, T., Dahlman, H., 1995. Precision, repeatability and validation of the localization of cranial landmarks using computed tomography scans. The Cleft Palate-Craniofacial Journal 32, 217–227.
Rosas, A., Bastir, M., 2002. Thin-plate analysis of allometry and sexual dimorphism in the human craniofacial complex. American Journal of Physical Anthropology 117, 236–245.

Shaffer, J.P., 1995. Multiple hypothesis testing. Annual Review of Psychology 46, 561–584.

Styner, M., Oguz, L., Xu, S., Brechbuehler, C., Pantazis, D., Levitt, J.J., Shenton, M.E., Gerig, G., 2006. Framework for the Statistical Shape Analysis of Brain Structures using SPHARM-PDM. ISC/NA-MIC Workshop on Open Science at MICCAI.

Theodore III, M.C., Richtsmeier, J.T., 1998. A simple method for visualization of influential landmarks when using Euclidean distance matrix analysis. American Journal of Physical Anthropology 107, 273–283.

Vidal, C.N., Nicolson, R., DeVito, T.J., Hayashi, K.M., Geaga, J.A., Drost, D.J., Williamson, P.C., Rajakumar, N., Sui, Y., Dutton, R.A., Toga, A.W., Thompson, P.M., 2006. Mapping corpus callosum deficits in autism: an index of aberrant cortical connectivity. Biological Psychiatry 60 (3), 218–225.

Wahl, M., Lauterbach-Soon, B., Hattingen, E., Jung, P., Singer, O., Volz, S., Klein, J.C., Steinmetz, H., Ziemann, U., 2007. Human motor corpus callosum: topography, somatotopy, and link between microstructure and function. The Journal of Neuroscience: The Official Journal of the Society for Neuroscience 27, 12132–12138.

Worz, S., Rohr, K., 2006. Localization of anatomical point landmarks in 3D medical images by fitting 3D parametric intensity models. Medical Image Analysis 10, 41–58.